Heliyon 9 (2023) e13312

Contents lists available at ScienceDirect

Heliyon

journal homepage: www.cell.com/heliyon

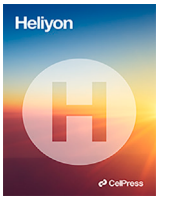

Research article

Identifying proxies and mapping heavy metals concentrations in city road dusts: A case study in the Brussels-Capital Region, Belgium

Patrick Bogaert [a,*], Gwenaël Diélie [b], Axel Briffault [a], Benoit de Saint-Hubert [a], Michel A. Verbanck [b]

[a] Earth & Life Institute, Université catholique de Louvain (UCLouvain), Belgium
[b] Department of Water Pollution Control, Université libre de Bruxelles (ULB), Belgium

ARTICLE INFO

Keywords:
Road dust
Heavy metals
Urban diffuse pollution
Traffic contaminants
Geospatial modeling
Spatial mapping

ABSTRACT

This paper investigates the spatial distribution of heavy metals (HMs) concentrations in road dusts over a part of the Brussels-Capital Region (BCR), with the aim of identifying the most relevant factors impacting these concentrations and subsequently mapping them over all road segments. For this goal, a set of 128 samples of road dusts was collected over a three years time span in the Anderlecht municipality, that covers about a tenth of the BCR area. The concentrations of Cd, Cr, Cu, Ni, Pb and Zn have been measured in the finest fraction ($\varnothing < 250$ μm) using ICP-OES. In parallel, continuous and categorical-valued proxies have been collected over all road segments. Using a multivariate linear modeling (MLR) approach, the most influential proxies that have been identified are the distance to the center of the BCR, land use, road hierarchy and roadside parking occupation. The performance of the MLR models remains however limited, with adjusted R^2 values around 0.5 for all HMs. From a spatial analysis of the regression residuals, it is likely that some useful proxies could have been overlooked. Although these models have clear limitations for reliably predicting HMs concentrations at specific locations, the corresponding maps drawn over all road segments provide a useful overview and help designing sound monitoring policies as well appropriate implementation of mitigation measures at places where road dust pollutants tend to concentrate. Further studies are needed to confirm this, but it is expected that our models will perform reasonably well over a large part of the BCR. It is believed too that our findings are relevant for modeling road dusts pollution in other cities as well.

1. Introduction

Environmental pollution in urban areas is a major and worldwide concern in medium to large cities. Since it impacts people's health and may cause serious environmental issues, it has gained considerable attention over the last decades. Atmospheric pollution related to fine particulate matter (PM) can mechanically impair lung function, but it impacts human physiology too due to the presence of polycyclic aromatic hydrocarbons (PAHs; [1–3]) and heavy metals (HMs; [4]).

* Corresponding author.
E-mail address: patrick.bogaert@uclouvain.be (P. Bogaert).

https://doi.org/10.1016/j.heliyon.2023.e13312
Received 8 September 2022; Received in revised form 30 November 2022; Accepted 26 January 2023

Available online 1 February 2023

Because of their toxicity and persistence, atmospheric and direct deposition of HMs is also a major concern [5]. HMs are mainly adsorbed on fine particles that accumulate from direct, wet and dry depositions on the road surfaces [6–8] and that are influenced by the urban surface properties in the roads vicinity [9–11]. As a result of urbanization, impermeable pavement is becoming ubiquitous in cities and it intensifies the accumulation of dust containing those pollutants [12]. Among non-exhaust sources, road dust resuspension has generally the highest impact on PM concentrations and is an increasing concern for air quality [13], especially within street canyons [14]. It has been shown that the finest polluted road sediment fractions can contaminate adults or children either by ingestion, by inhalation or by dermal absorption [15–18]. HMs primarily attached to road dust deposited on urban roads are of particular concern too in the urban water environment, since stormwater runoff transports them to receiving waters and degrades water quality [8,19–23], thus creating environmental and population health issues at places than can be located far away from their emission areas.

Road dust includes HMs originating from multiple sources [24,25], and [26] provided a list of the main sources of HMs in contaminated runoff water. They mainly relate to the various parts of the vehicles (brakes, tires and vehicle body [27–29]) and from combustion. Other identified sources are road equipment, buildings coating, industrial activities and land use [30,31]. For urban runoff, [32] provided loading estimates of Pb, Cu, Cd, and Zn from specific sources, this including vehicles parts and buildings.

The adverse impact of HMs in road dust has motivated scientists to pay increasing attention to their quantification and modeling [18,33,34]. This includes the identification of the most important factors that contribute to road dust build-up and HMs concentrations. Quantifying the relationship between HMs and these various factors is essential for risk management, but most of the past studies have only analyzed them qualitatively [29]. Identifying and ranking these factors in terms of influence is critical for implementing effective mitigation measures (including revised street sweeping strategies) and for protecting urban residents [12,19].

Spatial studies confirmed the combined influence of various factors by highlighting hot spots caused by major roads and industries [35,36]. They highlight too the need to account for the spatial variability in health risk assessment [12,18]. In spite of these general findings, spatial studies related to HMs concentrations in urban road dust are rather scarce and tend to focus on city or regional scales using kriging techniques (see, e.g., [37–40]). Spatially predicting HMs concentrations in road dust by relying on relevant environmental factors is a much less common approach [12,24]. To bridge this gap, this study aims at proposing a methodology for identifying the most relevant factors to be accounted for. Mapping afterwards these concentrations over the various road segments of the study area is expected to provide some insight about the spatial distribution of these pollutants and is a requirement for designing sound monitoring policies as well as for the appropriate implementation of mitigation measures at places where road dust pollutants tend to concentrate.

2. Material and methods

2.1. The Brussels-Capital Region and Anderlecht municipality

The Brussels-Capital Region (BCR) is located in the center of Belgium, covering an area of 161.4 km^2 with a population of 1.2 million. As the economic capital of Belgium and headquarters of the European institutions, the BCR is the most densely populated region of the country and is subject to important commuter traffic. In spite of these intense socioeconomic activities, the BCR includes about 18.5% of green areas spread over the whole region, along with a wide variety of urban conditions, ranging from residential (and even semi-rural areas along its borders) to industrial areas located close to its center along the Brussels-Charleroi canal. As most important cities, the BCR is facing pollution issues that cannot be attributed to point sources as for cities with locally intense industrial activities. Instead, pollution is more diffuse and is likely resulting from the joint effect of various factors that are hard to disentangle.

The BCR is segmented in 19 municipalities of various areas and populations. The Anderlecht municipality (AM) is the third biggest one and is located in its south-western part, extending from the densely populated inner ring area that encloses partly the City of Brussels to the much greener outer ring that encloses the whole BCR (Fig. 1). It covers 17.7 km^2 and has a population of 120,000 with an average population density of 6,800 km^{-2}. However, as for the whole BCR in general, it exhibits a strong gradient of population density between the inner ring (about 20,000 km^{-2}) and the outer ring (about 500 km^{-2}). The AM has an industrial and agricultural past reflected by its current land uses, with 34% of non built areas, 4% of industrial areas (mostly located along the Brussels-Charleroi canal), 36% of residential and densely populated areas, and 8% of areas related to public services. In the context of our study, the Anderlecht municipality (AM) was deemed representative of the whole BCR, as it includes about 10% of the BCR area and population, with varied urban conditions that are typically found in the BCR. It is thus expected that findings for the AM are likely to be relevant for the whole BCR.

2.2. Heavy metals sampling campaign and analyses

In order to investigate the concentrations of HMs in road dust, a total of 128 samples were collected and analyzed over 3 successive years between April and September during dry periods (i.e., a minimum of 24 hours after the last rain). The first 2019 sampling campaign collected 100 samples over road segments that were selected in order to keep a balance between spatial coverage over the whole AM and variety of the roads types that are typically found in the municipality (Fig. 2). The 2020 sampling campaign added 8 samples collected at two four-arms crossroads (where the four locations in each crossroad have similar characteristics) and 12 samples collected along distinct road transects. Finally, the 2021 sampling campaign added 8 more samples along the Brussels-Charleroi ship

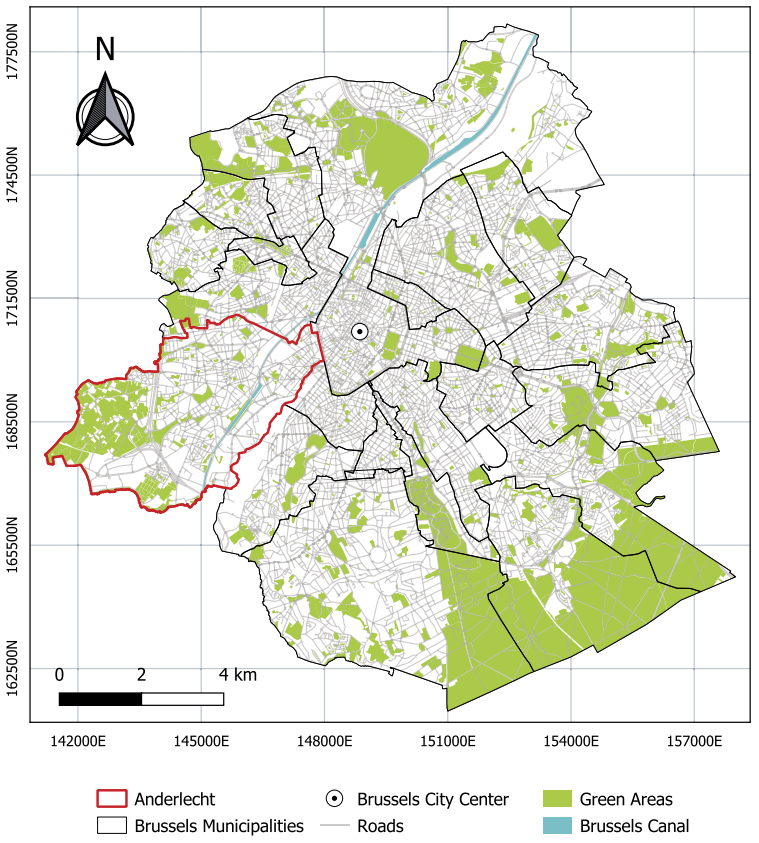

Fig. 1. Road network of the Brussels-Capital Region (in gray) with its green areas (colored in green) and location of the Anderlecht municipality (bounded in red). The blue curve refers to the Brussels canal crossing the region, the thick black curves correspond to the boundaries of the municipalities, while the disk refers to the center of the City of Brussels.

canal. The 100 samples of the 2019 campaign were used for the initial modeling, while the 2020 and 2021 additional samples were used for improving this modeling and for assessing the spatial independence of the prediction errors.

For all sampled locations, road dusts were collected over an area of 6 m^2 using an industrial-grade MAKITA (18V Li-ion 100 mbar DCL 501Z) vacuum cleaner. The bulk road dust samples were dried overnight in an oven at 50 °C. After that, sieving was performed (Analysette by FRITSCH) to remove the particles larger than 250 μm. The purpose of the sieving is to get rid of coarse objects (such as gravel, coarse sand, plant material and other debris such as plastic pieces and cigarette butts), all known to contribute significantly to the heterogeneous nature of street residues. The analysis of the heavy metals was conducted on the particle size fractions smaller than 250 μm, which are deemed sufficiently homogeneous and have consistently been demonstrated to contain the highest heavy metal levels in urban road dusts [34,41,42]. The choice of 250 μm as a particle-size cutting is also consistent with the prospect of developing optimized street sweeping practices suitable for moderately polluted urban environments [43].

The fraction smaller than 250 μm is recovered for the analysis of Cd, Cr, Cu, Ni, Pb and Zn. For each sediment analysis, one gram of the fraction is extracted in 10 ml aqua regia solution (HNO3:HCl = 1:3 v/v) for two hours at boiling state (heating plate programmed above 300 °C) in an Erlenmeyer flask placed under a water-refrigerated condensation column in a hood. This digestion strategy is derived from [30,44,45]. For each sample the extraction is performed three times (i.e., three consecutive one-gram subsampling) in order to reduce the intrinsic spatial heterogeneity of particulate contaminants. After the hot extraction, the mixture is filtered (filter n°1 by WHATMAN). The filter is rinsed and the extraction and rinsing liquids are added to Milli-Q quality water in a 50 ml volumetric flask. The solutions are then injected in the Inductively Coupled Plasma with an Optical Emission Spectrometry (ICP-OES vista pro by VARIAN). The various heavy metal concentrations (in mg/kg) are obtained by taking the average of the three (one-gram) replicas.

2.3. Spatial proxies

In parallel to the sampling campaigns, a large set of spatial proxies was collected for the road segments of the AM, with the aim of investigating their relationship with HMs concentrations. The term “proxies” refers here to influential factors that can directly impact HMs concentrations or to factors that are indirectly related to them. According to the fact that HMs concentrations are expected to result from the joint effect of several factors that are acting in a diffuse way over the BCR, the largest possible set

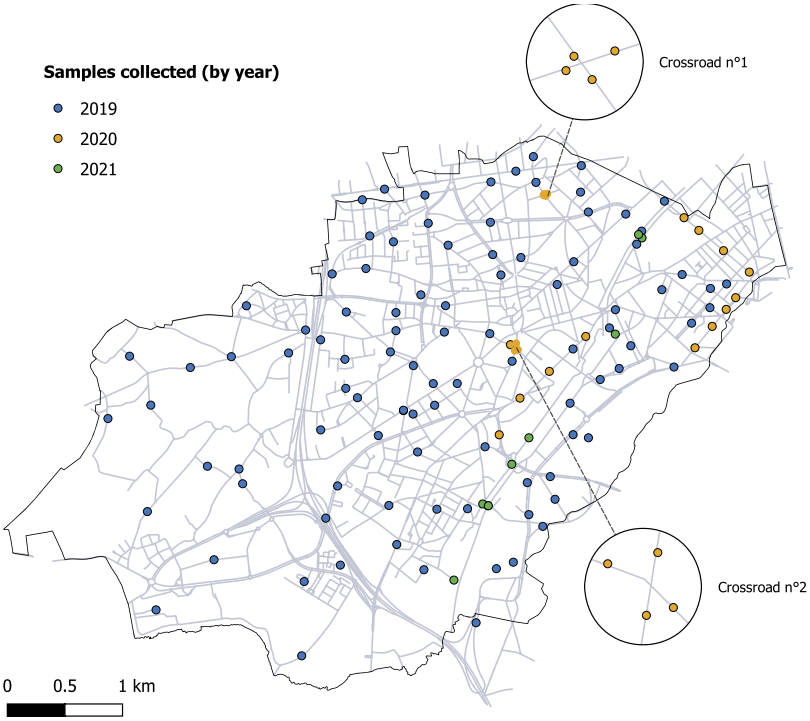

Fig. 2. Locations of the samples in the Anderlecht municipality, with the initial 100 samples in 2019 (in blue), the 20 additional samples in 2020 (in orange) and the 8 additional samples in 2021 (in green). The 8 locations sampled in two crossroads are highlighted in the zoomed parts of the figure.

of proxies was collected in order to cover aspects as various as socio-economy, demography, atmospheric pollution, meteorology, land use, traffic, road properties and road management. These proxies were gathered from various administrations and services, this including the Brussels agency for environment (Bruxelles Environnement, BE), the Brussels agency for mobility (Bruxelles-Mobilité, BM), the Royal Meteorological Institute (IRM), the Belgium National Institute for Statistics (IBSA), the IT service of the region (URBIS) and the Anderlecht municipality (AM). The list of all proxies is given in Table 1. These proxies are either continuous-valued or categorical-valued and are available at various initial spatial and temporal resolutions. As our goal was to map HMs concentrations over all road segments using these proxies, their value need to be known for all segments. Accordingly and whenever possible, all continuous-valued proxies have been spatially interpolated over all road segments using QGIS [46] and averaged over time when needed. On the other side, for categorical-valued proxies, Road coating type and Road condition were only available at the sampled locations and were not interpolated but were included in the analyses for the sake of completeness.

2.4. Proxies screening

Due to the large number of proxies at hand, screening methods were used to safely discard those that were not available for all road segments, as well as to identify the best subset of remaining ones to be used.

For the proxies that are at hand but which are either only known at the sample locations, are affected by missing values or cannot be extrapolated over all road segments, it is important to check that omitting them afterwards in the statistical analyses is not likely to negatively impact the subsequent results. A preliminary screening was done by assessing separately the importance of each proxy with respect to each HM. For continuous-valued proxies, simple linear regression models were used, while a one-way analysis of variance (ANOVA) was used for categorical-valued proxies. Statistical significance was tested in order to assess the impact that neglecting these proxies might have on the subsequent modeling stage.

2.5. Regression models

Based on all remaining proxies (i.e., after discarding those that are not known for all road segments), a multivariate linear regression (MLR) model was estimated separately for each HM, with the aim of selecting the best subset of proxies to be considered for predicting HMs concentrations, with

$$E[Y|x_1,\ldots,x_k] = \beta_0 + \beta_1 x_1 + \cdots + \beta_k x_k \tag{1}$$

where Y is the log-concentration of a given HM and where $x_1,\ldots,x_k$ are the k proxies included in the model. Proxies were selected using a forward selection procedure, where the statistical significance of each proxy was assessed using its p-value, while the

Table 1
List of the available spatial proxies. First part of the table refers to continuous-valued proxies, whereas second part refers to categorical-valued ones.

Proxy	Details	Unit	Provider
Distance to BCR center	center of BCR: Great Market place	km	URBIS
Crossroad distance	closest street node	m	URBIS
Black carbon	peak time, bulk time	$\mu g/m^3$	BE
Atmospheric pollutants	Cd, Cr, Cu, PM_{10}, $PM_{2.5}$	$\mu g/m^3$	BE
Street canyon index	average building height/street width	–	BE
Population density	by district	km^{-2}	IBSA
Road occupation rate	by district, 8-9 am and 17-18 am	–	ISBA
Roadside parking Occupation rate	by district, 5-7 am and 10-12 am	–	ISBA
Waterproof surface ratio	by district	–	ISBA
Buildings older than 1961	by district, ratio	–	IBSA
Number of shops	by district, per 1000 people	–	IBSA
Employment rate	by district	–	IBSA
Sedentary rate	by district	–	IBSA
Number of vehicles (MUSTI)	daily, rush hours	–	BM
Distance to shopping area	closest shopping area	m	BM
Average & total precipitation	week before sampling	mm	IRM
Average & total sun exposure	week before sampling	hours	IRM
Proxy	**Classes**	**Unit**	**Provider**
Road coating type	asphalt, pavement, mixture	–	samples
Road condition	new, good, degraded	–	samples
Speed Limit	30 km/h, 50 km/h, 70 km/h	–	URBIS
Land use	green area, densely populated, industrial, residential, mixed	–	URBIS
Road hierarchy	metropolitan road, main & interdistrict road, district collector & district road	–	BM
Regular Street Sweeping	yes, no	–	AM
Street Manager	municipality, region	–	AM

Legend: AM: Anderlecht municipality, BE: Bruxelles Environnement, BM: Bruxelles-Mobilité, IRM: Royal Meteorological Institute, ISBA: Belgium National Institute for Statistics, URBIS: IT service of the region, samples: obtained during the samples collection. The word "MUSTI" stands for the Strategic multimodal mobility model, operated by Bruxelles-Mobilité in the BCR. The word "district" refers to the 78 individual statistical sectors covering the total territory of the municipality of Anderlecht

performance of the regression models was assessed using the adjusted determination coefficient R_a^2 (i.e., the part of variance explained by the model), with

$$R_a^2 = 1 - \frac{RSS/(n-k-1)}{TSS/(n-1)} \tag{2}$$

where n is the number of samples, TSS is the total sum of squares and RSS is the residual sum of squares. Model selection was done using the Akaike's information criterion (AIC), with

$$AIC = n\ln(RSS/n) + 2(k+1) + C \tag{3}$$

where C is a constant that can be ignored for the sake of models comparison (see, e.g., [47] for more details). Both eqs. (2) and (3) where used jointly for selecting the best final model for each HM.

For each HM considered separately, a regression model was first estimated using the 100 samples of the 2019 campaign and was improved afterwards by including the additional samples from the 2020 and 2021 campaigns (see Section 2.6 below). For each HM, the proxies to be included in the MLR models were chosen using a forward selection procedure using the *ols_step_forward_aic()* function in R [48], with the goal of identifying the model that maximizes AIC, where included proxies are all statistically significant.

After estimating the final models that make use of all samples from the 2019, 2020 and 2021 campaigns, the potential benefit of including additional interactions terms $x_i x_j$ and quadratic terms x_i^2 was tested for all proxies appearing in these models. Finally, using for each HM the estimated MLR model, HMs concentrations were mapped over all road segments of the AM using QGIS [46], thus providing some insight about the spatial distribution of the HM concentrations over the municipality.

2.6. Repeatability and validation

As mentioned in Section 2.2, the first 2019 sampling campaign was conducted without having prior information about the most relevant proxies and their benefit for predicting HMs concentrations. Using the 100 samples from this first campaign, identifying these relevant proxies was possible and corresponding regression models were estimated. Using the additional samples from the 2020 and 2021 campaigns, several important points were addressed.

The first one was to check that the MLR models calibrated using data collected in 2019 are still relevant when applied for subsequent years. This implicitly assumes that HM concentrations are reasonably stable over time when no changes of proxies are taking place, so that the model estimated from the 2019 campaign will apply equally well for subsequent years. If this is verified,

Table 2
Main statistics for the n concentrations (in mg/kg) of the various HMs collected during the 2019 campaign (first part) and the 2020-2021 campaigns (second part).

$n = 98$	Cd	Cr	Cu	Ni	Pb	Zn
Min.	0.20	2.48	5.23	5.09	4.16	21.43
Median	2.69	82.07	159.41	41.25	75.46	330.99
Mean	2.66	94.98	210.74	47.83	117.39	353.55
Max.	6.71	473.24	1076.80	218.22	1671.75	1511.78
$n = 28$	Cd	Cr	Cu	Ni	Pb	Zn
Min.	1.71	49.58	46.68	26.18	47.24	163.32
Median	6.44	148.55	304.90	88.20	166.69	456.37
Mean	5.96	158.34	360.52	85.13	202.03	478.67
Max.	8.46	288.60	994.91	171.69	624.37	1018.95

this also offers the possibility to combine the 2019, 2020 and 2021 sampling campaigns in order to improve the estimation of the MLR model and the quality of the predictions. For a MLR model estimated from the 2019 campaigns and which is consistent with the observed values for the 2020 and 2021 campaigns, it is expected that, on the average, $(1-\alpha)100\%$ of the observed values for 2020 and 2021 will lie within the prediction intervals at the $1-\alpha$ confidence level. A value of $\alpha = 0.05$ was selected here for this purpose. More formally, if $n = 28$ is the number of predictions and m is the number of observed values that lie within their corresponding prediction intervals, this is equivalent to check that the frequency $f = m/n$ is compatible with the binomial distribution $Bi(n, p)$, where $p = 1-\alpha = 0.95$. Stated in other words, 0.95 should belong to the confidence interval for p delimited by the lower and upper bounds p_a and p_b when using f as an estimate of p.

The second point was to assess the spatial independence of the MLR residuals. As our study is accounting for a limited number of proxies, it can be suspected that there are other proxies that are impacting the HMs concentrations and that could have improved the MLR models if they were accounted for. The omission of a relevant proxy acting at a large scale would be translated by an apparent spatial correlation for the regression residuals. This motivated the 2020 sampling campaign that added 8 samples in two four-arms crossroads (where each crossroad is characterized by the same values for the proxies), so that the spatial dependence at very short distances can be estimated from them. More generally, the spatial dependence of the residuals can be measured using the semivariogram $\gamma(||\mathbf{h}||)$, defined as

$$\gamma(||\mathbf{h}||) = \frac{1}{2} Var[\varepsilon(\mathbf{x}+\mathbf{h}) - \varepsilon(\mathbf{x})]$$

where $\gamma(||\mathbf{h}||)$ is a measure of the dissimilitude between regression residuals $\varepsilon(.)$ at locations $\mathbf{x}$ and $\mathbf{x}+\mathbf{h}$ as a function of the euclidean distance $||\mathbf{h}||$ that separates them. For each HM, $\gamma(||\mathbf{h}||)$ was estimated and modeled using an exponential variogram model, i.e.

$$\gamma(||\mathbf{h}||) = \alpha_1 \delta_{(||\mathbf{h}||\neq 0)} + \alpha_2 (1 - \exp(-3||\mathbf{h}||/r)) \quad (4)$$

with $\delta_{(.)}$ the Kronecker delta (the nugget effect). Parameters α_1 and α_2 are associated with the spatially uncorrelated and correlated part of the residuals, respectively, where $\alpha_1 + \alpha_2$ is the variance of the residuals. Accordingly, $\alpha_2/(\alpha_1+\alpha_2)$ is measuring the part of the variance of the residuals that can be attributed to spatially correlated variations, while r (the range) is measuring the spatial extent of this correlation. More details about variogram estimation and modeling can be found in [49].

3. Results and discussion

3.1. Heavy metal distributions

The main statistics for the collected values are given in Table 2. Two samples from the 2019 sampling campaign were discarded due to abnormally high concentrations that can be related to their peculiar locations (close to a railroad and in a tunnel).

From a scatter plots analysis of the remaining samples (Fig. 3), it can be seen that all HM concentrations are reasonably close to normality after a logarithmic transform. All HMs are significantly correlated ($p_v \leq 0.01$). The highest correlation ($r = 0.92$) is observed for {Cr,Ni} that are jointly found in stainless steel. The lowest correlations are observed for {Cd,Cu} ($r = 0.62$), where Cd has the lowest correlations with other HMs in general and exhibit the lowest concentrations too. These correlations are consistent with those found by [31] and are in agreement with the fact that most of these HMs are directly linked to vehicles emissions. In agreement with [32], low Cd concentrations are expected as little Cd was found from any of the sources they evaluated, by comparison with other HMs.

From now on, as normality is easing both statistical analyses and visualization, all subsequent processing of the HMs concentrations will be based on their natural logarithm. The correspondence with the non transformed values will be provided when it comes to mapping the concentrations over the road segments of the municipality.

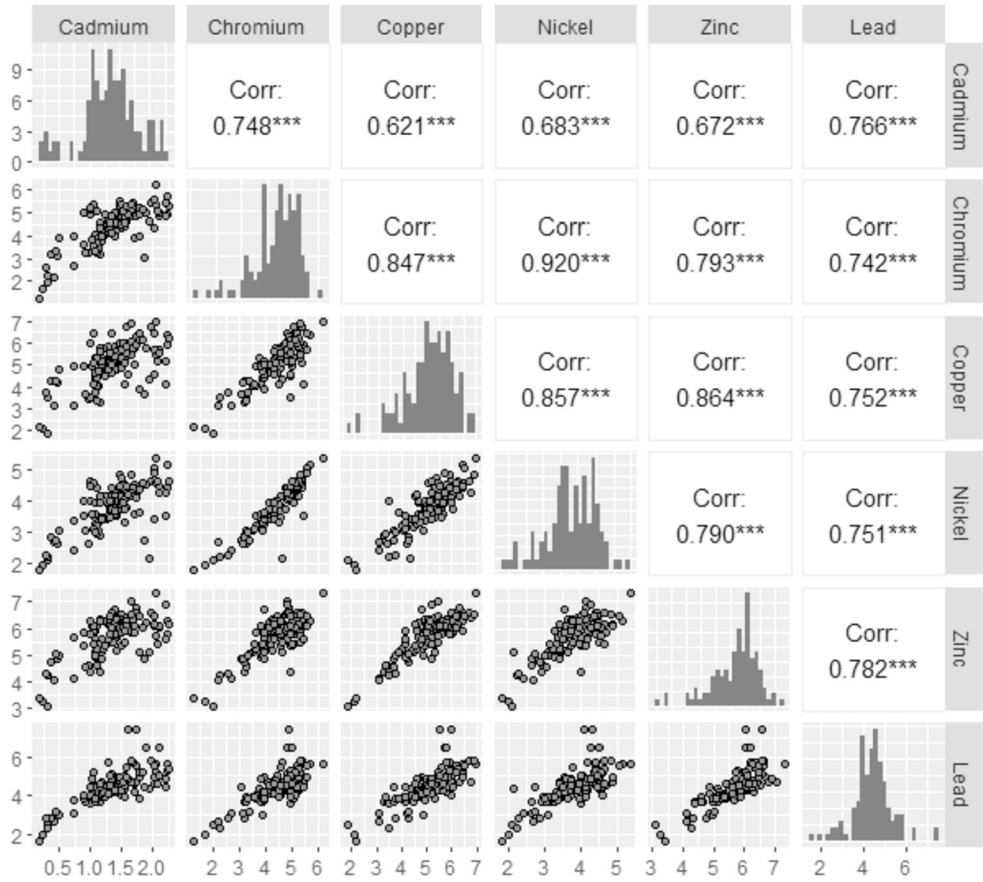

Fig. 3. Histograms for the 126 heavy metals concentrations (in natural logarithm), along with the corresponding scatter plots and correlations for all pairs.

3.2. Proxies screening

Table 3 presents the results for the individual screening of each proxy, where proxies affected by missing values (i.e., $n < 98$) are ranked in increasing order with respect to their mean p-value, while proxies that are only at hand at the sample locations (i.e., Road coating and Road condition) are presented at the bottom of the table. For the sake of comparison, the first part of the table presents the five most influential proxies.

From these results, it can be seen that proxies that cannot be used for predicting HMs concentrations over all road segments are lagging behind in terms of p-values (except for Employment rate), and most of them are not highly significant ($p_v > 0.01$) or are not significant at all ($p_v > 0.05$) for a majority of HMs. They can thus be safely omitted for the subsequent analyses. From a correlation analysis (details not shown here), it appears that Employment rate is correlated ($r = 0.85$) to Roadside parking occupation (10-12 am), a proxy which is at hand for all road segments. Discarding Employment rate is thus expected to have a limited impact, as its effect is indirectly accounted for by Roadside parking occupation.

3.3. Regression model and subsequent sampling campaigns

Based on the 98 samples from the 2019 campaign and using only the set of proxies that are known for all road segments, the best MLR model (i.e. the model that maximizes AIC) was estimated separately for each HM using the forward selection procedure (results not shown here). Based on these models and the knowledge of the values for the proxies at the sample locations for the 2020 and 2021 campaigns, the HMs concentrations at these locations were predicted and compared to the measured ones. For a MLR model estimated from the 2019 campaigns and which is consistent with the measured concentrations for the 2020 and 2021 campaigns, it is expected that, on the average, 95% of the 2020 and 2021 measurements will lie within the 0.95 prediction intervals. This was verified separately for each HM and the results are provided in Table 4. It can be seen that, except for Cd, this a reasonable assumption, so that it is possible to pool the data for all campaigns in order to redo the estimation of the MLR models with an increased number of samples, thus leading to a better estimation of these models. This also means that the global behavior of the HMs concentrations did not appear to change in a significant way over the three years time span covered by our study. As mentioned, this does not seem to be completely true for Cd, but it is worth remembering that Cd exhibits much lower concentrations by comparison with the other HMs (see Table 2), so that these measured concentrations are thus subject to a much higher relative analytical uncertainty. As

Table 3
p-values for the simple linear regression models (continuous proxies) and one-way ANOVA models (categorical proxies) that relate the concentration of each HM with each proxy. The first part refers to the five most influential proxies based on their mean p-value (denoted as $\overline{p_v}$); the second part refers to proxies that are impacted by missing values ($n < 98$); the third part refers to proxies that are only known at the sample locations. Proxies are sorted in increasing order of $\overline{p_v}$ in each part of the table.

Proxy	Cd	Cr	Cu	Ni	Pb	Zn	$\overline{p_v}$	n
Distance to BCR center	4.2e-5	2.3e-9	1.5e-9	1.3e-10	1.2e-8	2.3e-13	7.0e-6	98
Roadside parking occupation (5-7am)	5.4e-4	5.9e-5	1.5e-6	4.6e-5	1.4e-4	3.7e-7	1.3e-4	98
Land use	9.3e-4	4.3e-5	5.6e-9	9.0e-5	5.4e-6	8.7e-9	1.8e-4	98
Waterproof surface ratio	3.9e-3	2.2e-6	1.0e-8	6.6e-7	9.9e-6	1.4e-10	6.5e-4	98
Distance to shopping area	0.022	1.4e-5	5.7e-8	2.4e-5	4.0e-3	2.9e-7	4.0e-3	98
Employment rate	5.1e-4	4.14e-3	9.8e-4	3.4e-3	1.2e-4	4.0e-4	1.6e-3	78
Speed limit	1.6e-3	0.013	6.7e-3	0.055	0.026	7.7e-3	0.018	95
Road occupation rate	0.048	0.093	5.4e-3	0.039	0.119	0.013	0.053	44
Street Manager	0.058	0.020	0.016	6.6e-3	0.306	0.026	0.072	93
Atmospheric pollutants (Cu)	0.149	0.168	0.281	0.067	0.024	0.022	0.118	87
Atmospheric pollutants (Cr)	0.318	0.264	0.437	0.132	0.061	0.038	0.208	87
Atmospheric pollutants (Ni)	0.251	0.295	0.275	0.247	0.185	0.047	0.217	87
Road occupation rate (17-18 am)	0.376	0.069	0.117	0.267	0.444	0.220	0.249	96
Sedentary rate	0.952	0.326	7.0e-3	0.221	0.891	0.041	0.406	78
Road occupation rate (8-9 am)	0.616	0.121	0.246	0.321	0.836	0.460	0.433	96
Road coating	0.138	7.4e-3	8.8e-3	0.021	0.134	0.099	0.068	98
Road condition	0.327	0.868	0.329	0.408	0.012	0.125	0.346	98

Table 4
Number of values m lying within the corresponding 95% prediction intervals and corresponding frequencies $f = m/n$ for the $n = 28$ predictions at the sample locations for the 2020 and 2021 campaigns, along with the lower and upper bounds p_a and p_b of the confidence interval for the probability p of the binomial distribution $Bi \sim (n, p)$. HMs for which $p_a \leq 0.95 \leq p_b$ corresponds to the non rejection of the null hypothesis $p = 0.95$ (at the confidence level 0.99).

	Cd	Cr	Cu	Ni	Pb	Zn
m	21	28	27	27	28	25
f	0.75	1	0.96	0.96	1	0.89
p_a	0.49	0.83	0.76	0.76	0.83	0.66
p_b	0.92	1.00	1.00	1.00	1.00	0.99

Table 5
Selected proxies ($p_v \leq 0.05$) for the MLR models, with their corresponding p-values. Last two lines give the adjusted R^2 values for the corresponding models and for models that additionally include statistically significant ($p_v \leq 0.05$) quadratic and interaction terms (where no additional terms are significant for Cd).

Proxy	Cd	Cr	Cu	Ni	Pb	Zn
Distance to BCR center	2.7e-2	5.4e-3	–	1.3e-8	1.7e-5	2.6e-7
Land use	5.0e-2	9.0e-3	4.2e-5	–	1.8e-2	8.0e-4
Road hierarchy	1.0e-2	1.0e-3	5.4e-4	3.6e-3	–	–
Roadside parking occupation (5-7am)	4.2e-5	2.5e-4	–	4.4e-2	4.9e-3	–
Street canyon index	–	–	2.8e-2	4.9e-3	1.6e-2	–
Population density	3.5e-2	6.0e-4	–	–	–	–
Roadside parking occupation (10-12am)	1.9e-2	–	–	–	–	–
Black carbon (peak time)	–	–	–	–	1.7e-2	–
R_a^2 (models given above)	0.45	0.50	0.51	0.48	0.48	0.49
R_a^2 (with higher terms)	0.45	0.54	0.54	0.54	0.55	0.53

processing Cd differently from the other HMs would largely complicate the subsequent processing steps, it was decided to proceed without specific corrections for this issue.

Accordingly, Table 5 presents the final MLR models that account for all sampling campaigns together. Overall, all R_a^2 values are close to 0.5, showing that only half of the variability is explained by these MLR models, with a slightly lower values for Cd. However, this is better than R^2 values reported by [24] in a comparable study for predicting Cd, Cr, Cu, Ni, and Pb concentrations using a set of 66 proxies in Tianjin, China.

Using the number of times each proxy is involved for the various HMs, it is seen that Distance to BCR center and Land use seem to be the most relevant ones (5 HMs out of 6), followed by Road Hierarchy and Roadside parking occupation from 5 to 7 am (4 HMs out of 6). Road Hierarchy and Land use proxies were expected to be relevant by reference to previous studies. Indeed, road hierarchy

Table 6
Values of the coefficients for the MLR models. The intercept corresponds to the hypothetical expected (log-)concentration for a location at the center of the city, in a green area and on a district collector & district road with null Roadside parking occupation. Proxies are unitless except when mentioned between brackets.

Coefficients	Cd	Cr	Cu	Ni	Pb	Zn
Intercept	1.541	4.708	3.412	4.862	5.460	5.963
Distance to BCR center [km]	-0.096	-0.208	–	-0.271	-0.324	-0.235
Land use : Densely populated	0.086	0.688	1.442	–	0.623	0.783
Land use : Industrial	0.128	0.951	1.568	–	0.348	0.858
Land use : Mixed	0.334	0.836	1.463	–	0.733	0.882
Land use : Residential	0.044	0.522	0.815	–	0.162	0.456
Road hierarchy : Metropolitan	0.279	0.475	0.947	0.439	–	–
Road hierarchy : Main, Interdistrict	0.205	0.500	0.504	0.335	–	–
Roadside parking occupation (5-7 am)	-0.011	-0.017	–	-0.005	-0.011	–
Street canyon index	–	–	0.749	0.497	0.549	–
Population density [km^{-2}]	2.36e-5	6.99e-5	–	–	–	–
Roadside parking occupation (10-12 am)	7.22e-3	–	–	–	–	–
Black carbon (peak time) [$\mu g/m^3$]	–	–	–	–	0.100	–

is linked to expected traffic and land uses are associated with various levels of human activities, that have been shown to impact HMs concentrations in road deposits [30,31,34,36]. E.g., using a more limited set of proxies, [19,29] concluded that spatial variation of HMs concentrations could be attributed to the variability in pollutant sources such as traffic and land use.

It is worth remembering here that the non significance of a proxy for some HMs does not prove that this proxy should be discarded for these HMs, but rather that the data failed to clearly evidence its effect. This could be linked to a mild effect of this proxy on the HMs concentrations, and it is an expected issue too when low signal-to-noise ratio occurs, as highlighted by the moderate R_a^2 values of our MLR models. Accordingly, the interpretation of the results should thus be conducted at the global level instead of interpreting them separately for each HM, by remembering that all HMs are correlated and are thus expected to be impacted in comparable ways by similar proxies.

The estimated coefficients of the MLR models are given in Table 6, by considering the Green area class and the District collector/road class as the reference classes for Land use and Road Hierarchy, respectively (i.e., their associated coefficients are equal to 0). Whenever significant, it can be seen that HMs concentrations decrease when moving away from the center of the city, as expected from the spatial organization of the AM and BCR in general. This is consistent with the findings by [50], who related this gradient to increasing traffic in the most central urban areas, while [51] reported that metal pollutants are related to anthropogenic activities, with road traffic being an important contributor.

By comparison with the Green area reference class, it is clear too that other land uses lead to increased concentrations, with the highest increase observed for Cu. In general, the Industrial and Mixed classes lead to the highest increases, while Residential areas leads to the smallest ones. This is consistent too with the findings by [41,52,53] in China, that reported industrial area roads dust as the most polluted ones. However for our study, even if the contrast with Green areas is clear, the differences between other land use classes are more limited and vary between HMs. This is in agreement with the fact that only few production industries are still active in the BCR, and those that are in activity are subject to strict environmental controls. Most of the differences are thus expected to come from traffic intensity.

Looking now at the impact of Road Hierarchy, whenever significant, the coefficients emphasize that larger roads lead to higher concentrations by comparison with the reference class, but differences between metropolitan and Main & interdistrict roads are limited, except for Cu. Similarly, [36] reported that the spatial patterns observed for Cu, Pb, Cr and Zn were mainly associated with main roads with high traffic density, thus suggesting that these concentrations are directly related to vehicles emissions, as expected. Moreover, larger roads are associated with heavy vehicle traffic, and these vehicles are characterized by braking systems and combustion emissions that largely differ from those for standard cars.

Whenever significant too, Roadside parking occupation rate (5-7 am) consistently evidence a negative impact on concentrations. This is in agreement with the fact that high occupation rates before working hours are mainly associated with dense urban residential areas. On the other side, Street canyon index has a consistently positive impact, in agreement with the fact that high street canyon index values are associated with conditions that locally concentrate atmospheric pollutants, while [5,8] highlighted the relationship between atmospheric deposition and HMs concentrations in road dusts.

For other proxies, they can hardly be interpreted as they are significant for only one or two HMs. It is worth emphasizing that Population density does not seem to have a clear impact, while [31] evidenced it. However, this proxy is related to a large extent to the distance to the center of BCR, which is clearly impacting the concentrations.

Overall, it can be concluded that all proxies that were identified as relevant for most of the HMs lead to consistent results for these HMs and are also in agreement with their expected effects as documented from previous studies. However, it can be seen too that evidencing their effect for all HMs at the same time is a much more difficult task, most likely due to our limited samples size and a low signal-to-noise ratio.

So far, our MLR models (as given in eq. (1)) only include linear effect with respect to each proxy, while including curvatures (i.e. quadractic terms) and interactions could potentially improve them. For each HM, the statistical significance of these terms was thus tested. The corresponding results (not detailed here) show that, for all HMs, a total of 11 quadratic and interaction terms (out of 49 possible terms) are statistically significant ($p_v \leq 0.05$). However, the involved proxies largely differ between HMs, thus impairing the

Table 7
Estimation of the spatially correlated part of the MLR residuals, as measured by the ratio $\alpha_2/(\alpha_1+\alpha_2)$, where $\alpha_1+\alpha_2$ corresponds to the variance of these residuals.

	Cd	Cr	Cu	Ni	Pb	Zn
$\frac{\alpha_2}{\alpha_1+\alpha_2}$	0.24	0.81	0.26	0.63	0.53	0.38

global interpretation of these terms. Moreover, only 5 of these terms are highly significant ($p_v < 0.01$). As seen from Table 5 (last line), accounting for these additional terms does not substantially modify the predictive performance of the regression models, as measured by the moderate increase of the R_a^2 values. Accordingly, they were not accounted for predicting HMs concentrations over the road segments of the AM. This also eases the interpretation of the MLR and the corresponding maps, as the result corresponds to the summation of the separate effect for each proxy.

3.4. Mapping HMs concentrations

Using the road network of the AM as presented in Fig. 2 along with the estimated MLR as given in combined Tables 5 and 6, it was possible to map the predicted HMs concentrations over all road segments of the municipality, except for segments that are associated with land use classes that were not represented in our samples (namely "Administrative activity" and "Transport & port activity"), along with the "Highway" road hierarchy class that cannot be safely sampled. For the sake of brevity, the corresponding maps in Figs. 4a and 4b are presented here for Cu and Zn only because these two HMs exhibit the most distinct patterns. As Zn concentrations were modeled by accounting for the Distance to the center or BCR and for Land use, they exhibit a linear gradient with few locally contrasting areas that are associated with distinct land use classes (with only Green areas and Residential areas that markedly differ from the other ones; see last column in Table 6). As green areas are mostly located in the West part of the municipality (see Fig. 1) and are the most distant ones from the center of the region, the corresponding expected concentrations are particularly low over the Western road segments. The map of predicted Cu concentrations shows similarly low values in the Western part, but the local variations in the Eastern part are more complex and pronounced, due to the inclusion of Road Hierarchy and Street canyon index as additional proxies for that metal (see third column in Table 6). It is worth noting that even if Cu does not explicitly account for the Distance to the center of the BCR, concentrations are still globally higher on the Eastern part (i.e. close to the center), as observed for the other HMs. The maps for these other HMs (that are presented in Figs. 6a to 6d in the Appendix) share the same general behavior.

It is worth emphasizing here that mapping HMs concentrations in urban areas is usually done on a regular spatial grid, either using kriging or other interpolation techniques from a set of sampled locations (e.g., [4,17,38,40,53]) or using regression models with gridded values for the proxies, as long as the values of the proxies are known everywhere [24]. On the opposite, mapping was done here on a road-segment basis. The benefit of this approach is that very local variations between adjacent road segments can be evidenced when these segments are characterized by distinct values of land use, road hierarchy, roadside parking occupation, etc. This mapping is also more consistent with monitoring policies and with the implementation of mitigation measures (such as enhanced street sweeping modes), as specific road segments can be targeted for these goals. It is however a more demanding approach, as the values for the proxies need to be known for all road segments.

3.5. Spatial dependence of the regression residuals

In order to assess the spatial dependence of the regression residuals, variograms were estimated for all HMs and were modeled using eq. (4). The corresponding results for Cr and Cu are shown in Figs. 5a and 5b, respectively, while the estimation of the spatially correlated part is given in Table 7 for all HMs. It can be seen from Fig. 5 that these residuals are spatially correlated up to a distance of about 700 meters, but the amount of this correlation largely varies between HMs, with moderate values $\alpha_2/(\alpha_1+\alpha_2)$ for Cd and Cu but a high value for Cr. Based on these results, it is thus likely that our MLR models could be improved by including spatially correlated proxies that have been overlooked in our study. From the fact that regression residuals are all positively correlated between HMs (results not shown here), with correlations ranging from 0.24 to 0.81 (average value is 0.52), it is likely too that these omitted proxies would affect all HMs in similar ways. On the other side, for the spatially non correlated part of the residuals, it emphasizes that concentrations can be subject to large variations over small distances, as caused by very local effects that are difficult to identify at the scale of our study due to the limited number of samples collected over the spatial extent of the municipality. Overall, the part of this unexplained residual variability (either spatially correlated or uncorrelated) as measured by $\alpha_1+\alpha_2$ is about 50% for all HMs, as previously mentioned and seen from Table 5. However, it is worth remembering that a very detailed mapping of the concentrations would bring little benefits from an environmental perspective and for management aspects at the scale of the municipality, while the additional experimental costs required for this mapping would be overwhelming.

4. Conclusions

In this paper, we investigated the spatial distribution of various HMs concentration in the smallest fraction ($\varnothing < 250$ μm) of road dusts collected over the Anderlecht municipality in the Brussels-Capital Region, that covers about 18 km^2 and that can be considered as representative of the whole region. Based on a three years sampling campaign, it has been shown that the main proxies (among

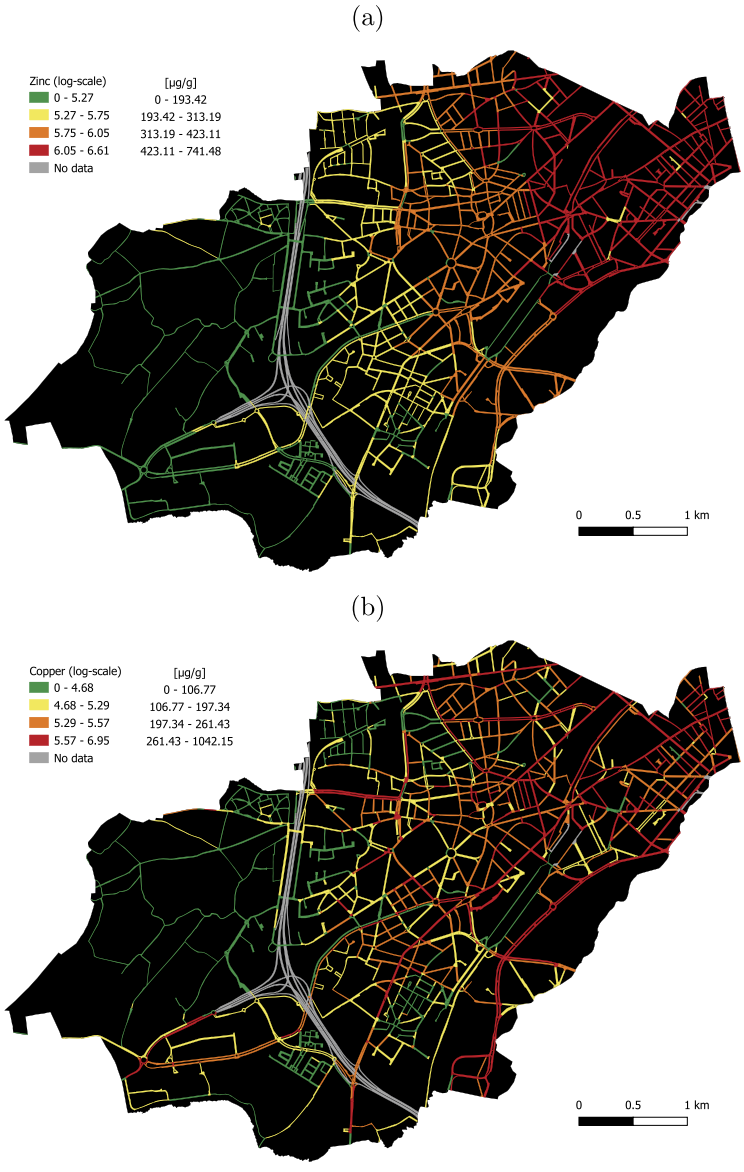

Fig. 4. Predicted Zn (part a) and Cu (part b) concentrations over the road segments of the Anderlecht municipality, based on the corresponding estimated MLR models. Concentrations are presented in four classes that correspond to the quartiles of the distribution of the predicted concentrations. Limits for the quartiles are given both in log-scale and original values. The few "No data" road segments correspond to two Land use classes and one Road hierarchy class that were not represented in the samples.

those that were at hand) that best relate to these concentrations are the distance to the center of the region, land use, road hierarchy and roadside parking occupation before working hours. The predictive performance of the corresponding multivariate regression models remains limited for all HMs, as half of the variance is left unexplained. From a spatial analysis of the regression residuals, it can be suspected that relevant spatial proxies could have been omitted, though their identification is not possible in the framework of this study. Using these models for accurately predicting local HMs concentrations is thus not possible, but the corresponding maps of expected concentrations over the municipality give a useful overview when it comes to improve street cleaning management at the municipality level, either by identifying hot spots or by sorting areas in terms of priority.

From the results obtained here for a single municipality in the region, it is expected that the same model could be applied for other municipalities as well, without requiring new extensive sampling campaigns. Indeed, our samples cover a wide range of conditions with respect to the proxies that were identified as relevant. However, further targeted sampling is required in order to account for specific land use, i.e., few areas of intense transport and port activities that were not represented in the municipality but that are occurring in other parts of the region, and where typical concentrations are expected to be higher too. In parallel, it is expected that improved results could be obtained by using proxies that are available at a higher spatial resolution. Indeed, due to the limited spatial resolution of several proxies that were used in this study, most of them were interpolated to various extents and in different

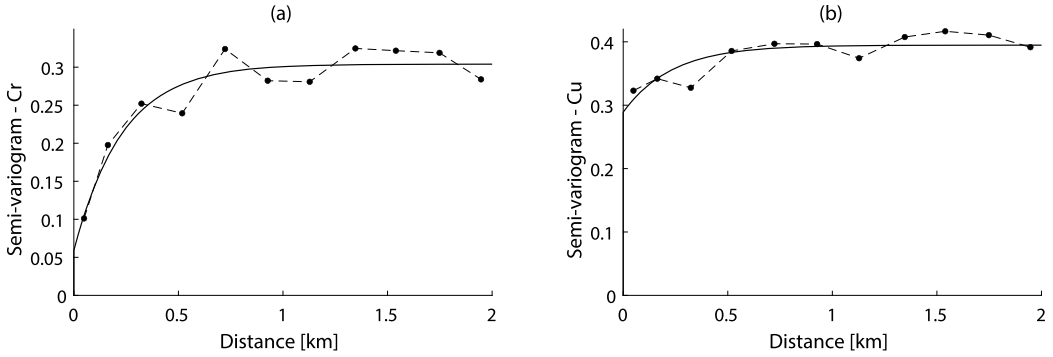

Fig. 5. Semivariograms of the regression residuals for Cr and Cu. Dashed lines correspond to the estimated semivariograms while plain lines correspond to the fitted exponential models. For each model, the intercept is equal to α_1 while the plateau corresponds to the variance $\alpha_1 + \alpha_2$.

ways over the road segments of the municipality. As these interpolations lead to reduced performance for the regression models, a line of action is to improve the databases of the Brussels-Capital Region in order to provide spatially more detailed information, thus limiting the impact of such approximations.

By comparing the evolution of the HMs concentrations over the three years time span, it can be tentatively concluded that they are not subject to major changes over time, as long as one is focusing on the finest fraction of the road dusts. As far as it is feasible, attention should however be paid to collecting samples in similar weather conditions and over the shortest possible time period in order to limit the effect of physico-chemical processes (transport and runoff in combination with sorption and desorption processes) that might negatively impact the comparability of these concentrations over time. Further studies that aim at tracking and modeling the dynamics of HMs concentrations at few locations would obviously increase the ecological and management value of such models. Doing so would help to quantify both the accumulation rate of HMs in road dusts over time and the proportion of these HMs that is removed during runoff events.

In spite of all aforementioned limitations, it is believed that our study is beneficial for other ongoing studies in this field of research, as it offers guidelines for the selection and improvement of the most relevant proxies and for mapping HMs concentration in other cities, as long as adaptations are made in order to account for their specificities, of course.

Funding statement

Professor Patrick Bogaert and Professor Michel A. Verbanck were supported by Innoviris-2019-BRIDGE-GOLEM Project.

CRediT authorship contribution statement

Patrick Bogaert; Gwenaël Diélie; Axel Briffault; Michel A. Verbanck: Conceived and designed the experiments.
Gwenaël Diélie: Performed the experiments.
Patrick Bogaert; Gwenaël Diélie; Axel Briffault; Benoit de Saint-Hubert; Michel A. Verbanck: Analyzed and interpreted the data.
Patrick Bogaert; Axel Briffault; Michel A. Verbanck: Wrote the paper.

Declaration of competing interest

The authors declare no competing interests.

Data availability

Data will be made available on request.

Acknowledgement

The authors thank the Anderlecht Municipality for its help in the course of the project, and their colleagues Alexandre Van Baekel, Julien Schneider and Benoît Dochy who provided technical assistance.

Appendix A. Maps of predicted concentrations for Cd, Cr, Ni and Pb

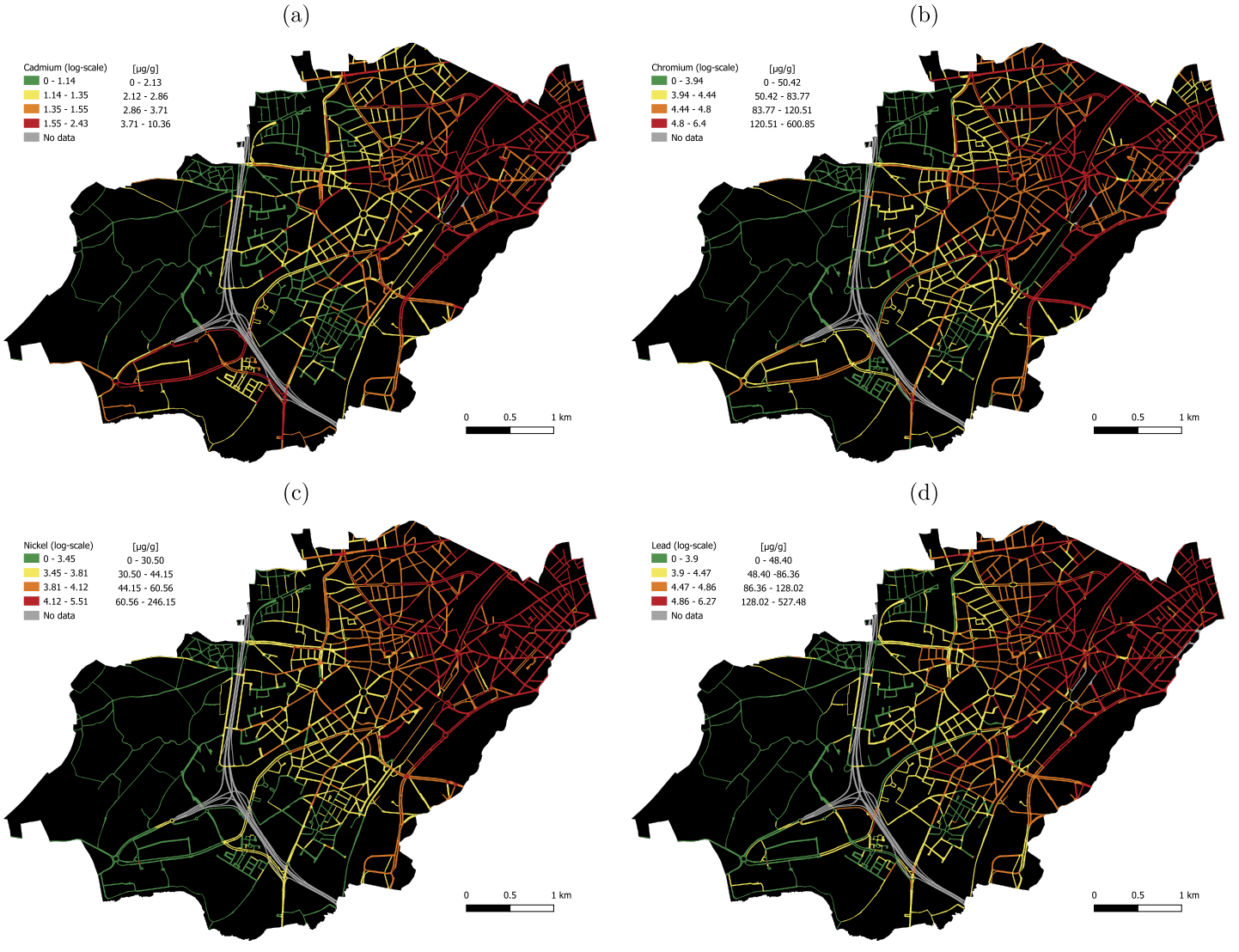

Fig. 6. Predicted concentrations of (a) Cd, (b) Cr, (c) Ni and (d) Pb over the road segments of the Anderlecht municipality, based on the corresponding estimated MLR models. Concentrations are presented in four classes that correspond to the quartiles of the distribution of the predicted concentrations. Limits for the quartiles are given both in log-scale and original values. The few "No data" road segments correspond to two Land use classes and one Road hierarchy class that were not represented in the samples.

References

[1] A. Guilbert, K. De Cremer, B. Heene, C. Demoury, R. Aerts, P. Declerck, O. Brasseur, A.V. Nieuwenhuyse, Personal exposure to traffic-related air pollutants and relationships with respiratory symptoms and oxidative stress: a pilot cross-sectional study among urban green space workers, Sci. Total Environ. 649 (2019) 620–628, https://doi.org/10.1016/j.scitotenv.2018.08.338.

[2] B. Skrbić, N. Durišić-Mladenović, J. Živančev, D. Tadić, Seasonal occurrence and cancer risk assessment of polycyclic aromatic hydrocarbons in street dust from the Novi Sad city, Serbia, Sci. Total Environ. 647 (2019) 191–203, https://doi.org/10.1016/j.scitotenv.2018.07.442.

[3] G. Wang, Y. Wang, W. Yin, T. Xu, C. Hu, J. Cheng, J. Hou, Z. He, J. Yuan, Seasonal exposure to pm2.5-bound polycyclic aromatic hydrocarbons and estimated lifetime risk of cancer: a pilot study, Sci. Total Environ. 702 (2020) 115005, https://doi.org/10.1016/j.scitotenv.2019.135056.

[4] K. Cai, C. Li, S. Na, Spatial distribution, pollution source, and health risk assessment of heavy metals in atmospheric depositions: a case study from the sustainable city of Shijiazhuang, China, Atmosphere 10 (2019) 222, https://doi.org/10.3390/atmos10040222.

[5] A. Liu, Y. Ma, J. Gunawardena, P. Egodawatta, G. Ayoko, A. Goonetilleke, Heavy metals transport pathways: the importance of atmospheric pollution contributing to stormwater pollution, Ecotoxicol. Environ. Saf. 164 (2019) 696–703, https://doi.org/10.1016/j.ecoenv.2018.08.072.

[6] C. Samara, D. Voutsa, Size distribution of airborne particulate matter and associated heavy metals in the roadside environment, Chemosphere 59 (8) (2005) 1197–1206, https://doi.org/10.1016/j.chemosphere.2004.11.

[7] Q. Wang, M. Liu, Y. Li, Y. Liu, S. Li, R. Ge, Dry and wet deposition of polycyclic aromatic hydrocarbons and comparison with typical media in urban system of Shanghai, China, Atmos. Environ. 144 (2016) 175–181, https://doi.org/10.1016/j.atmosenv.2016.08.079.

[8] L. Zhang, M. Gao, J. Cui, F. Yang, H. Wang, C. Fu, Y. Huang, Wet deposition of trace metals at a typical urban site in Southwestern China: fluxes, sources and contributions to aquatic environments, Sustainability 10 (2017) 69, https://doi.org/10.3390/su10010069.

[9] M. Legret, C. Pagotto, Heavy metal deposition and soil pollution along two major rural highways, Environ. Technol. 27 (2006) 247–254, https://doi.org/10.1080/09593332708618641.

[10] N. Ghanavati, A. Nazarpour, B. De Vivo, Ecological and human health risk assessment of toxic metals in street dusts and surface soils in Ahvaz, Iran, Environ. Geochem. Health 41 (2018) 875–891, https://doi.org/10.1007/s10653-018-0184-y.

[11] A. Christoforidis, N. Stamatis, Heavy metal contamination in street dust and roadside soil along the major national road in Kavala's region, Greece, Geoderma 151 (2009) 257–263, https://doi.org/10.1016/j.geoderma.2009.04.016.

[12] H. Wang, C. Shen, Y. Kang, Q. Deng, X. Lin, Spatial distribution of pollution characteristics and human health risk assessment of exposure to heavy elements in road dust from different functional areas of Zhengzhou, China, Environ. Sci. Pollut. Res. 27 (2020) 26650–26667, https://doi.org/10.1007/s11356-020-08942-7.

[13] E. Padoan, F. Ajmone-Marsan, X. Querol, F. Amato, An empirical model to predict road dust emissions based on pavement and traffic characteristics, Environ. Pollut. 237 (2018) 713–720, https://doi.org/10.1016/j.envpol.2017.10.115.

[14] O. Brasseur, P. Declerck, B. Heene, P. Vanderstraeten, Modelling black carbon concentrations in two busy street canyons in Brussels using CANSBC, Atmos. Environ. 101 (2015) 72–81, https://doi.org/10.1016/j.atmosenv.2014.10.049.

[15] M. Gabarron, A. Faz, J. Acosta, Soil or dust for health risk assessment studies in urban environment, Arch. Environ. Contam. Toxicol. 73 (2017) 442–455, https://doi.org/10.1007/s00244-017-0413-x.

[16] A. Torghabeh, A. Jahandari, R. Jamasb, Concentration, contamination level, source identification of selective trace elements in Shiraz atmospheric dust sediments (Fars Province, SW Iran), Environ. Sci. Pollut. Res. 26 (2019) 6424–6435, https://doi.org/10.1007/s11356-018-04100-2.

[17] A. Bourliva, C. Christophoridis, L. Papadopoulou, K. Giouri, A. Papadopoulos, E. Mitsika, K. Fytianos, Characterization, heavy metal content and health risk assessment of urban road dusts from the historic center of the city of Thessaloniki, Greece, Environ. Geochem. Health 39 (2016) 611–634, https://doi.org/10.1007/s10653-016-9836-y.

[18] F. Li, J. Zhang, J. Huang, D. Huang, J. Yang, Y. Song, G. Zeng, Heavy metals in road dust from Xiandao District, Changsha City, China: characteristics, health risk assessment, and integrated source identification, Environ. Sci. Pollut. Res. 23 (2016) 131100–131113, https://doi.org/10.1007/s11356-016-6458-y.

[19] A. Liu, C. Gunawardana, J. Gunawardena, P. Egodawatta, G.A. Ayoko, A. Goonetilleke, Taxonomy of factors which influence heavy metal build-up on urban road surfaces, J. Hazard. Mater. 310 (2016) 20–29, https://doi.org/10.1016/j.jhazmat.2016.02.026.

[20] H. Hwang, M. Fiala, D. Park, T. Wade, Review of pollutants in urban road dust and stormwater runoff: part 1. Heavy metals released from vehicles, Int. J. Urban Sci. 20 (3) (2016) 334–360, https://doi.org/10.1080/12265934.2016.1193041.

[21] H. Hwang, M. Fiala, D. Park, T. Wade, Review of pollutants in urban road dust and stormwater runoff: part 2. Organic contaminants from vehicles and road management, Int. J. Urban Sci. 23 (4) (2019) 445–463, https://doi.org/10.1080/12265934.2018.1538811.

[22] J. Gunawardena, P. Egodawatta, G. Ayoko, A. Goonetilleke, Atmospheric deposition as a source of heavy metals in urban stormwater, Atmos. Environ. 68 (2013) 235–242, https://doi.org/10.1016/j.atmosenv.2012.11.062.

[23] H. Zhao, J. Zhao, C. Yin, X. Li, Index models to evaluate the potential metal pollution contribution from washoff of road-deposited sediment, Water Res. 59 (2014) 71–79, https://doi.org/10.1016/watres.2014.04.012.

[24] X. Yuan, T. An, B. Hu, J. Zhou, Analysis of spatial distribution characteristics and main influencing factors of heavy metals in road dust of Tianjin based on land use regression models, Environ. Sci. Pollut. Res. (2022) 1–12, https://doi.org/10.1007/s11356-022-22151-4.

[25] R. Han, B. Zhou, Y. Huang, X. Lu, S. Li, N. Li, Bibliometric overview of research trends on heavy metal health risks and impacts in 1989–2018, J. Clean. Prod. 276 (2020) 123249, https://doi.org/10.1016/j.jclepro.2020.123249.

[26] S. Meland, Management of contaminated runoff water: current practice and future research needs, Technical Report, Conférence Européenne des Directeurs des Routes, 2016.

[27] F. Fujiwara, R.J. Rebagliati, L. Dawidowski, D. Gómez, G. Polla, V. Pereyra, P. Smichowski, Spatial and chemical patterns of size fractionated road dust collected in a megacity, Atmos. Environ. 45 (2011) 1497–1505, https://doi.org/10.1016/j.atmosenv.2010.12.053.

[28] R. Harrison, A. Jones, J. Gietl, J. Yin, D. Green, Estimation of the contributions of brake dust, tire wear, and resuspension to nonexhaust traffic particles derived from atmospheric measurements, Environ. Sci. Technol. 46 (12) (2012) 6523–6529, https://doi.org/10.1021/es300894r.

[29] Y. Ma, S. Mummullage, B. Wijesiri, P. Egodawatta, J. McGree, G.A. Ayoko, A. Goonetilleke, Source quantification and risk assessment as a foundation for risk management of metals in urban road deposited solids, J. Hazard. Mater. 408 (2021) 124912, https://doi.org/10.1016/j.jhazmat.2020.124912.

[30] T. Duong, B. Lee, Partitioning and mobility behavior of metals in road dusts from national-scale industrial areas in Korea, Atmos. Environ. 43 (2009) 3502–3509, https://doi.org/10.1016/j.atmosenv.2009.04.036.

[31] J. Trujillo-González, M. Torres-Mora, S. Keesstra, E. Brevik, R. Jiménez-Ballesta, Heavy metal accumulation related to population density in road dust samples taken from urban sites under different land uses, Sci. Total Environ. 553 (2016) 636–642, https://doi.org/10.1016/j.scitotenv.2016.02.101.

[32] A. Davis, M. Shokouhian, S. Ni, Loading estimates of lead, copper, cadmium, and zinc in urban runoff from specific sources, Chemosphere 44 (5) (2001) 997–1009, https://doi.org/10.1016/S0045-6535(00)00561-0.

[33] H. Chen, X. Lu, L. Li, Spatial distribution and risk assessment of metals in dust based on samples from nursery and primary schools of Xi'an, China, Atmos. Environ. 88 (2014) 172–182, https://doi.org/10.1016/j.atmosenv.2014.01.054.

[34] T. Duong, B. Lee, Determining contamination level of heavy metals in road dust from busy traffic areas with different characteristics, J. Environ. Manag. 92 (2011) 554–562, https://doi.org/10.1016/j.jenvman.2010.09.010.

[35] S. Charlesworth, M. Everett, R. McCarthy, A. Ordonez, E. de Miguel, A comparative study of heavy metal concentration and distribution in deposited street dusts in a large and a small urban area: Birmingham and Coventry, West Midlands, UK, Environ. Int. 29 (2003) 563–573, https://doi.org/10.1016/S0160-4120(03)00015-1.

[36] B. Wei, F. Jiang, X. Li, S. Mu, Spatial distribution and contamination assessment of heavy metal in urban road dusts from Urumqui, NW China, Microchem. J. 93 (2) (2009) 147–152, https://doi.org/10.1016/j.microc.2009.06.001.
[37] K. Irvine, M. Perrelli, R. Ngoen-klan, I. Droppo, Metal levels in street sediment from an industrial city: spatial trends, chemical fractionation, and management implications, J. Soils Sediments 9 (2009) 328–341, https://doi.org/10.1007/s11368-009-0098-5.
[38] H. Pan, X. Lu, K. Lei, A comprehensive analysis of heavy metals in urban road dust of Xi'an, China: contamination, source apportionment and spatial distribution, Sci. Total Environ. 609 (2017) 1361–1369, https://doi.org/10.1016/j.scitotenv.2017.08.004.
[39] C. Men, R. Liu, F. Xu, Q. Wang, L. Guo, Z. Shen, Pollution characteristics, risk assessment, and source apportionment of heavy metals in road dust in Beijing, China, Sci. Total Environ. 612 (2018) 138–147, https://doi.org/10.1016/j.scitotenv.2017.08.123.
[40] V. Kolakkandi, B. Sharma, A. Rana, S. Dey, P. Rawat, S. Sarkar, Spatially resolved distribution, sources and health risks of heavy metals in size-fractionated road dust from 57 sites across megacity Kolkata, India, Sci. Total Environ. 705 (2020) 135805, https://doi.org/10.1016/j.scitotenv.2019.135805.
[41] X. Bi, S. Liang, X. Li, A novel in situ method for sampling urban soil dust: particle size distribution, trace metal concentrations, and stable lead isotopes, Environ. Pollut. 177 (2013) 48–57, https://doi.org/10.1016/j.envpol.2013.01.045.
[42] C. Lanzerstorfer, Heavy metals in the finest size fractions of road-deposited sediments, Environ. Pollut. 239 (2018) 522–531, https://doi.org/10.1016/j.envpol.2018.04.063.
[43] J. German, G. Svensson, Metal content and particle size distribution of street sediments and street sweeping waste, Water Sci. Technol. 46 (2002) 191–198, https://doi.org/10.2166/wst.2002.0679.
[44] F. Kabiadayi, H. Cesur, Determination of Cu, Pb, Zn, Ni, Co, Cd, and Mn in road dusts of Samsun City, Environ. Monit. Assess. 168 (2010) 241–253, https://doi.org/10.1016/j.envpol.2018.04.063.
[45] P. Marín Sanleandro, A. Sánchez Navarro, E. Díaz-Pereira, F. Bautista Zuñiga, M. Romero Muñoz, M.J. Delgado Iniesta, Assessment of heavy metals and color as indicators of contamination in street dust of a city in SE Spain: influence of traffic intensity and sampling location, Sustainability 10 (2018), https://doi.org/10.3390/su10114105.
[46] QGIS Development Team, QGIS Geographic Information System, QGIS Association, 2022, https://www.qgis.org.
[47] K. Burnham, D. Anderson, Model Selection and Multimodel Inference: A Practical Information-Theoretic Approach, 2nd ed., Springer-Verlag, New York, 2002.
[48] R Core Team, R: A Language and Environment for Statistical Computing, R Foundation for Statistical Computing, Vienna, Austria, 2017, https://www.R-project.org/.
[49] N. Cressie, Statistics for Spatial Data, revised ed., Wiley-Interscience, Hoboken (NJ), 2015.
[50] E. Apeagyei, M. Bank, J. Spengler, Distribution of heavy metals in road dust along urban-rural gradient in Massachusetts, Atmos. Environ. 45 (13) (2011) 2310–2323, https://doi.org/10.1016/j.atmosenv.2010.11.015.
[51] L. Tijhuis, B. Brattli, O. Saether, A geochemical survey of topsoil in the city of Oslo, Norway, Environ. Geochem. Health 24 (1) (2002) 67–94.
[52] H. Khademi, M. Gabarrón, A. Abbaspour, S. Martínez-Martínez, A. Faz, J. Acosta, Environmental impact assessment of industrial activities on heavy metals distribution in street dust and soil, Chemosphere 217 (2019) 695–705, https://doi.org/10.15666/aeer/1802_33313347.
[53] J. Li, X. Zhu, W. Yu, Y. Yu, Particle size, spatial variation, and pollution source apportionment of street dust from a typical industrial district, in Wuhan, China, Appl. Ecol. Environ. Res. 18 (2) (2020) 3331–3347, https://doi.org/10.15666/aeer/1802_33313347.